Multibeam Scanning Antenna System Based on Beamforming Metasurface for Fast 5G NR Initial Access

LUCA STEFANINI[1], **ALBERTO RECH**[2], **(Graduate Student Member, IEEE),**
DAVIDE RAMACCIA[1], **(Senior Member, IEEE), STEFANO TOMASIN**[2], **(Senior Member, IEEE),**
ALESSANDRO TOSCANO[1], **(Senior Member, IEEE), FEDERICO MORETTO**[3],
AND FILIBERTO BILOTTI[1], **(Fellow, IEEE)**

[1]Department of Industrial, Electronic and Mechanical Engineering, Roma Tre University, 00146 Rome, Italy
[2]Department of Information Engineering, University of Padova, 35122 Padua, Italy
[3]NTT Data Italia, 20143 Milan, Italy

Corresponding author: Luca Stefanini (luca.stefanini@uniroma3.it)

ABSTRACT Fifth-generation (and beyond) networks are characterized by ever more demanding requirements in terms of speed, bandwidth, and number of servable users. Fast and reliable access to the main network is mandatory, requiring technologies and procedures that ensure high performing cell search and initial access (IA). Existing phased array antennas (PAAs) are limited by the single beam scanning approach and complex feeding systems. In this paper, a beamforming metasurface that shifts the field manipulation from an electric level to an electromagnetic one is proposed for speeding up the IA procedure with respect to a traditional system using PAAs. The main advantage is given by the simultaneous transmission of multiple signals in different directions. The numerical results demonstrate that a much faster IA with similar success probability can be reached. Our system provides high gain, parallel computation, and scalability for larger systems, becoming a relevant candidate in the new radio and smart electromagnetic environment context.

INDEX TERMS New radio, millimeter waves, advanced antenna system, metasurfaces, beamforming, initial access.

I. INTRODUCTION

Fifth-generation (5G) [1], [2] and sixth-generation (6G) [3], [4] wireless systems will redefine the way we think about the radio environment. In this context, having a fast and reliable access to the main network is of paramount importance and requires technologies and procedures that ensure high performing cell search (CS) and initial access (IA). To accomplish these requirements, antenna systems must exhibit, among other characteristics, high directivity to overcome the limitations induced by the path loss typical of millimeter waves (mm-Waves). Consequently, scanning the space domain with a search procedure becomes mandatory to establish a link between the gNodeB (gNB) base station and user equipment (UE). This is a shift with respect to

The associate editor coordinating the review of this manuscript and approving it for publication was Giovanni Angiulli.

the 4G-LTE technology, where omni-directional antennas were used [5], and introduces additional latency. The reduction of the IA time has been a subject of several studies, mostly aiming at optimizing the set of directions explored by the gNB [6], [7].

The most prominent technology to obtain the required performances is Phased-Array Antennas (PAAs) [8], [9] and their declination of Unconventional-Phased-Array antennas (UPAAss) [10], [11]. A PAA consists of a set of multiple antennas fed *ad-hoc* through a Beamforming Network (BFN) that enables the shaping of the radiated beampattern. BFNs can be divided into two categories, *i.e.*, analog and digital: the former solutions consist of tunable phase shifters and power dividers, as schematically shown in Fig.1a; the latter solution uses a micro-controller system to modify the feeding signals at each antenna, as shown in Fig.1b, removing the need of RF components between transmitter and antenna, but

introducing drawbacks related to the processing unit. A different solution that embraces the best from both approaches is the matrix-BFN technology [12]–[14]. Its architecture consists of a complex microwave network of carefully engineered lines and power splitters, realizing a multiport device, able to radiate specific output beams according to the specific input port fed, as shown in Fig.1c. The matrix network solution offers great advantages in the CS and IA procedures: the ports are independent and can be used in parallel, radiating simultaneously a number of directive beams in the antenna Field-of-View (FoV). This configuration realizes a virtual wide-angle high-gain gNB that allows replicating in 5G technology a configuration similar to the one used in the 4G IA procedures [15], with the advantage of being much faster than its digital counterpart. Unfortunately, matrix BFNs become exponentially more complex for high gain applications, such as the gNB of 5G wireless systems, requiring many antennas. To continue benefitting from the advantages of matrix BFNs also in such a scenario, a different approach and a suitable enabling technology are required.

In this paper, we investigate the possibility to implement a matrix BFN at the electromagnetic level by using a properly designed *refractive metasurface (MTS).* The metasurface is an add-on device to be placed on top of a set of independent antennas, as schematically shown in Fig. 1d. In the proposed radiating system, each antenna can be connected to the radio-frequency (RF) chain through a selector (series), or one RF chain per antenna can be used (parallel). When a single antenna is radiating, the MTS transforms the illuminating field in a directive beam towards a specific direction. Different beams are radiated by selecting different antennas. Each beam can be radiated independently by feeding an antenna at a time, or simultaneously by activating all the antennas at once. The goal of this paper is to demonstrate that the IA procedures can be significantly speeded up thanks to a beamforming MTS. Thus, after having designed the beamforming MTS and evaluated its radiation and scanning pattern, we compare its ability to perform the IA procedure with a conventional implementation based on a BFN. When operating according to the third-generation partnership project (3GPP) standard, scanning the FoV with a single beam achieves a similar probability of success and time of the IA. However, the proposed MTS beamforming solution allows the simultaneous transmission of multiple signals in different directions. Therefore, we consider it as an improvement of the IA procedure that can be adopted in future evolutions of the standard, achieving a much faster IA with similar success probability. This is also confirmed by the extensive simulation results reported in this paper.

The rest of paper is organized as follows. Section II is devoted to the design of the scanning antenna system based on matrix beamforming MTS. In Section III, we report the comparison between the numerically computed radiation patterns of a conventional scanning antenna system and the proposed solution under different illumination conditions of
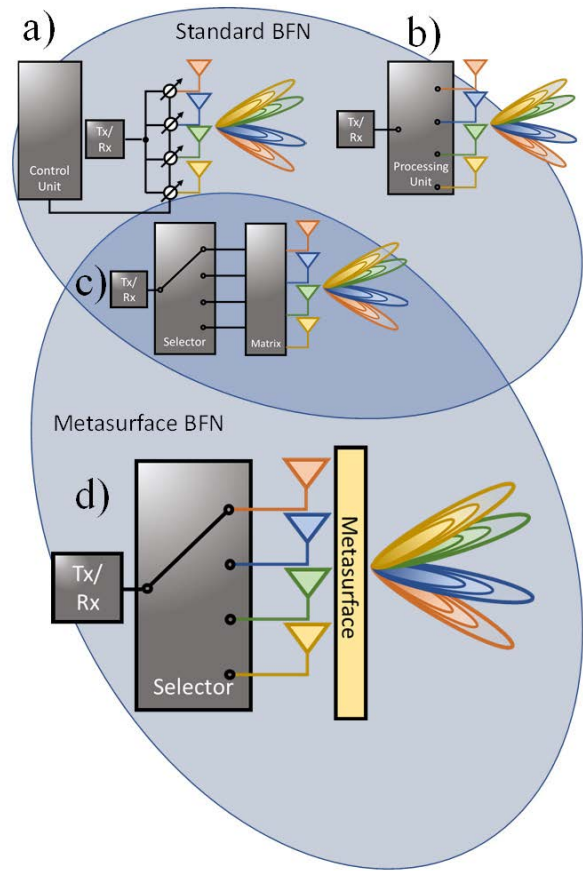

FIGURE 1. Sketches of the different architectures used for implementing BFNs: (a) analog BFN, (b) digital BFN, (c) matrix BFN, and (d) proposed MTS-based beamforming network.

the metasurface. In Section IV, the 3GPP IA procedure for 5G New Radio (NR) wireless systems is reported. The downlink and uplink IA performance of both BFN-based and MTS-based solutions is assessed and compared in Section V. Finally, Section VI draws the conclusion of the paper.

II. DESIGN OF THE SCANNING ANTENNA SYSTEM BASED ON MATRIX BEAMFORMING MTS

In this Section, we describe the design process of the proposed antenna system, composed by a properly designed refractive MTS and a set of antennas. MTS technology has rapidly captured the interest of scientists and engineers due its unprecedented ability to manipulate the electromagnetic field in a straightforward manner and with a low-cost implementation at microwaves and mm-Waves [16]. In recent years, both antenna technology and propagation environment have benefitted from the MTS technology, allowing the design of novel antenna systems for satellite and mobile scenarios [17]–[22], and defining the so-called smart electromagnetic environment based on intelligent MTSs [23]–[26].

The unprecedented ability to manipulate the electromagnetic field is given by the peculiar arrangement of the unit-cells composing the MTS. Indeed, a MTS is a planar

array of subwavelength artificial particles, whose scattering properties can be designed at will [27]. At the beginning, the scientific research has been mainly focused on engineering the properties of the periodic and passive MTSs (*Metasurfaces 1.0*) through a proper design of the unit-cell and the unit-cell spacing and interaction [28]. Then, the control over the properties of the MTSs has been enhanced at first by introducing spatial modulation (*Metasurface 2.0*) [18], [29] and, more recently, by exploiting temporal modulation (*Metasurface 3.0*) [30]–[34]. These generations of MTSs can be properly designed to operate in reflection or transmission. In our scenario, as described in Fig. 2, the MTS must be designed to efficiently transmit the electromagnetic field beyond it. Thus, we focus our attention on refractive MTSs, also known as Huygens MTS [29], [35]–[37], able to impart a point-to-point wavevector manipulation to the incident field to transform it into a desired phase-front. In combination with the antenna system, refractive MTSs enable several new features not achievable otherwise.

A. ANALYTICAL DERIVATION OF THE METASURFACE SPATIAL PROFILE

The required transformation can be described as follows: *the spherical wave radiated by each antenna must be transformed into a plane wave pointing into a specific direction according to the position of the antenna itself.* Therefore, the MTS should exhibit simultaneously two characteristics: 1) rectification of the spherical phase-front illuminating the metasurface into a refracted plane wave with the lowest possible insertion loss, and 2) steering the transmitted plane wave into different directions according to the relative position of the antenna within the array.

Let us consider a linear array of N independent antennas equally spaced, as shown in Fig. 2. The figure describes the geometrical configuration under analysis: the MTS is located at $z=0$ and it is theoretically infinitely extended in the x and y directions. Although the antenna array is just one row of the entire bidimensional array composing the gNB, a pair of periodic boundary conditions at $\pm y$-direction can be imposed for restoring the behaviour of the single row as if it were in the complete antenna. This strategy allows to significantly simplify the analysis but maintaining the theoretical and numerical results comparable with the ones obtained considering the full bidimensional array. Indeed, as well-known from the antenna array theory [38], this configuration relaxes the analysis to a single scanning plane. The illuminating antennas are aligned along the x direction at $(y = 0, z = -d)$ and an antenna at $x=x_0$ is radiating an electromagnetic field at frequency f_0. The domain is divided into two sub-domains, named Region 1 and 2, respectively, where the electromagnetic field generated and radiated by antenna ($\mathbf{E}_1$), and the one radiated by MTS ($\mathbf{E}_2$) are propagating. In case of lossless and totally refracting MTS, no reflected field is expected in Region 1 and the amplitudes of the fields in Region 1 and Region 2 are the same.
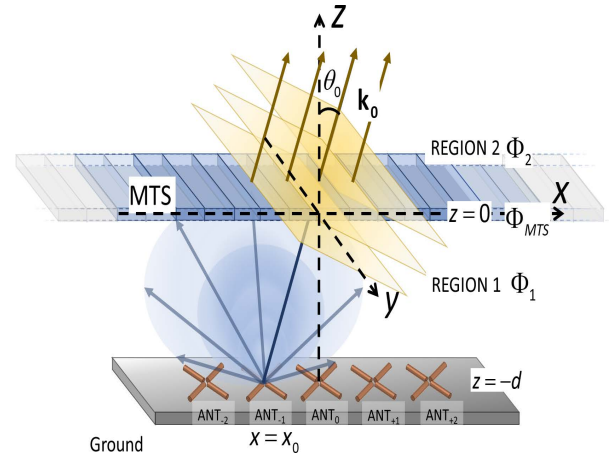

FIGURE 2. 3D sketch of a y-directed slice of the antenna system: an antenna array is placed above a metallic plate at distance -d from the metasurface placed at the origin of the reference system, (x=0, z=0, y=0). A spherical wave-front emerging from an element of the array laying in x=x₀, region 1, impinges on the metasurface and each block imprints a different phase-shift to obtain a plane wave along the θ₀ direction in region 2.

Under these assumptions, the field radiated by the antenna is:

$$\mathbf{E}_1(x, z) = \mathbf{E}_0 e^{-jk_0 r}, \text{ where } r = \sqrt{(x - x_0)^2 + (z + d)^2}, \tag{1}$$

where $k_0 = 2\pi/\lambda$ is the wavenumber at the design wavelength $\lambda_0 = c/f_0$, being c the speed of light in free space. The refracted field by the MTS in Region 2 is:

$$\mathbf{E}_2(x, z) = \mathbf{E}_0 e^{-jk_0 z \cos(\theta_0)} e^{-jk_0 x \sin(\theta_0)}, \tag{2}$$

where the pointing direction θ_0 is identified as the angle between the positive z-direction and the line passing through the origin of the axis and the active antennas, leading to:

$$\theta_0 = \tan^{-1}(x_0/d) \tag{3}$$

From (1) and (2) we note that the refracted field by the MTS in Region 2 can be obtained if the field phase distribution $\Phi_1(x)$ illuminating the MTS from Region 1 is modified to exhibit the field phase distribution $\Phi_2(x)$ of the refracted field in Region 2. Hence, the phase distribution of Region 1 combined with the one impressed by the MTS, $\Phi_{MTS}(x)$, must be equal to the phase distribution of Region 2. This can be written as follows:

$$\Phi_{MTS}(x) + \Phi_1(x, 0^-) = \Phi_2(x, 0^+)$$
$$\Phi_{MTS}(x) + k_0\sqrt{(x - x_0)^2 + d^2} = k_0 x \sin\theta_0. \tag{4}$$

From (4) we can obtain the spatially varying phase distribution of the transmission coefficient along the x-direction of the desired Matrix BF MTS:

$$\Phi_{MTS}(x) = k_0 x \sin\theta_0 - k_0\sqrt{(x - x_0)^2 + d^2}. \tag{5}$$

Equation (5) describes the optimum profile of the MTS that resembles the one of a perfect focusing lens used in optics,

where both nonlinear phase profile and angular dispersion are exhibited.

The implementation of such a complex profile using a refractive MTS is not straightforward task, especially for what concerns the engineering of the angular dispersion. However, for small values of x_0, the contribution of the sine function in (5) can be neglected, leading to a simple sub-optimal spatially varying phase profile of our matrix BF MTS:

$$\Phi_{MTS}(x) \approx -k_0\sqrt{x^2 + d^2}, \tag{6}$$

where x_0 has been neglected under the current assumptions. Equation (6) describes a phase profile of the transmission coefficient of the MTS that can be easily implementable as demonstrated in the next Sections. However, before moving towards the design, in the next Section we will derive the effect of such an approximation on the performance of the beamforming MTS.

B. OPERATIVE LIMITS OF SUB-OPTIMAL BEAMFORMING MTS

The approximations introduced on the spatially varying phase profile of the beamforming MTS are the main cause of the performance deterioration under different illumination conditions. However, for small values of x_0 close to $x = 0$, we expect that the optimal and the sub-optimal MTSs have similar performances, as discussed earlier. Therefore, now we derive the maximum value of x_0 giving performance comparable to the value of the optimum profile. This is of fundamental importance for defining the maximum FoV of the antenna system, as x_0 is related to the pointing angle θ_0 through (3). Furthermore, we derive the source characteristics to improve the sub-optimal MTS. In the following, we consider two different configurations for the antenna system: in the first configuration the MTS is located at distance $d = 2\lambda_0$ from the antenna array, while the distance in increased to $d = 5\lambda_0$ in the latter. Moreover, we limit the MTS in the x direction, fixing its extension to D, so that the position x_0 of the antenna can be referred to this maximum value.

In Fig. 3a-b, we report the optimum phase distribution described by (5) as a function of the normalized position x/D along the MTS and the normalized position of the antennas x_0/D for $d = 2\lambda_0$ and $d = 5\lambda_0$, respectively. Here, the angular dispersive property of the optimum profile is clearly visible: cutting the plot for different values of x_0/D returns different phase profiles along x/D. Fig. 3c-d, shows the sub-optimal phase distribution described by (6), for $d = 2\lambda_0$ and $d = 5\lambda_0$, respectively. Being (6) independent on the antenna position, the MTS phase profile is constant for any value of x_0/D. Finally, in Fig. 3e-f, the difference between the optimal and sub-optimal phase distribution for the two cases is shown, i.e., the error introduced by the sub-optimal profile. The two figures can be interpreted as an eye diagram: the wider the central area (the eye), the more similar are the sub-optimal and optimal MTS performances over the FoV. The error-free region, the eye, can be identified with the
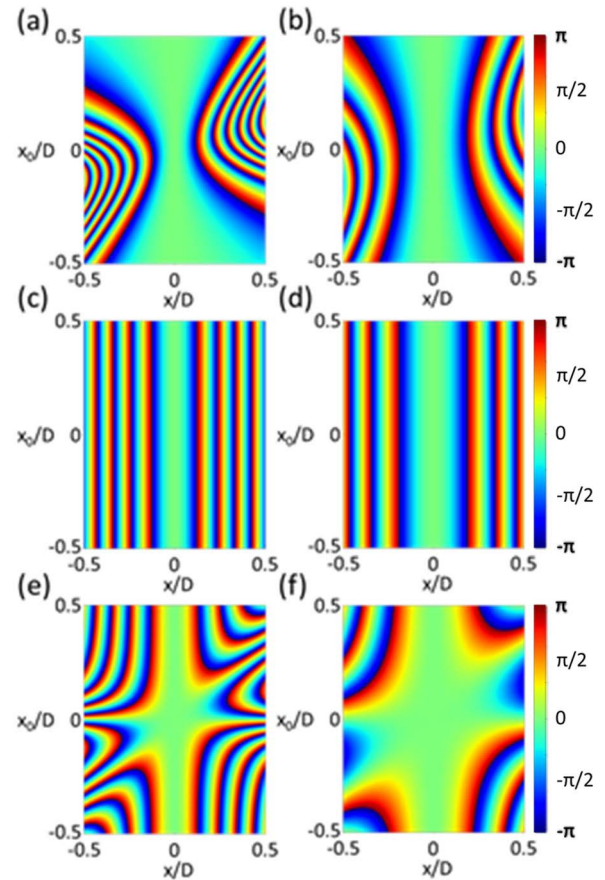

FIGURE 3. (a) and (b) Phase profiles for the optimum-profile, (c) and (d) Phase profiles for the sub-optimum profile, (e) and (f) their difference as phase-error. The distance between antennas and mts is (Left column) $d = 2\lambda$ and (Right column) $d = 5\lambda$.

small-angle approximation, already used for obtaining (6), i.e., $\tan(\theta) = \sin(\theta) = \theta$, that is valid for illumination angular beamwidth of $\pm 30°$ [39]–[41]. The shrinking of the beamwidth is obtained by managing the illumination pattern from the antenna array. By activating more than one antenna element simultaneously, we adjust the Half-Power-Beam-Width (HPBW) and, consequently, shrink the region of the MTS we are illuminating in a relevant way. Fig. 4 illustrates this process. If D_{max} is the maximum dimension of the region we can illuminate, identified by the white box in Fig.4, the condition we must satisfy derives from the validity of the small-angle approximation:

$$\begin{cases} D_{max} \ll d(1 + \theta_0) \\ \frac{x_0}{d} = \tan(\theta_0) \approx \theta_0. \end{cases} \tag{7}$$

From (7), we notice that positioning the antennas further away, i.e., increasing d, from the MTS enhances the performance, as discussed earlier and reported in Fig.4e-f. In the limit case of $\theta_0 = 30° = \pi/6$, we retrieve the highest value of x_0 as:
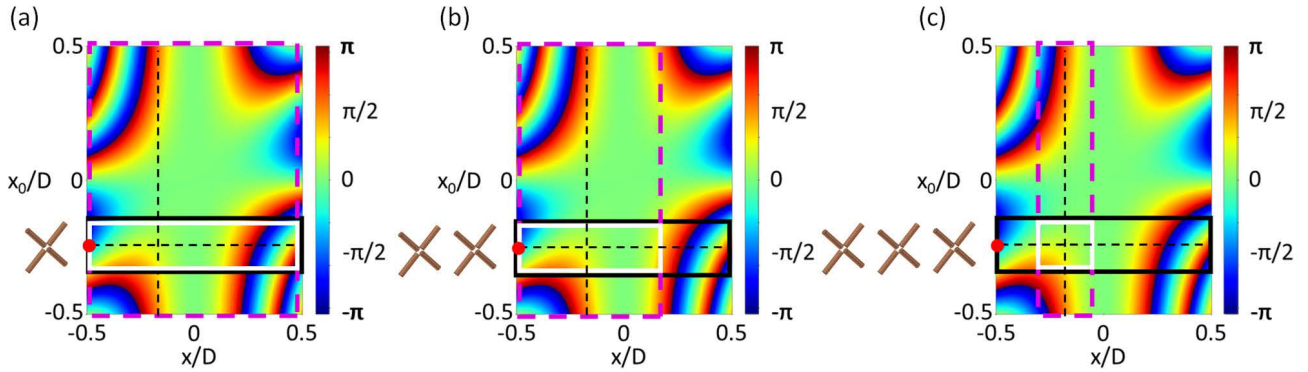
$$x_0 = d(\pi/6) \approx 0.52d, \tag{8}$$

FIGURE 4. Phase error accumulation by the refracted wave in region 2 when (a) one, (b) two and (c) three antennas are simultaneously active. The black box indicates the area occupied by the antenna, the pink box indicates the half-power-beam-width (HPBW) of the crossed-dipole and the white box stands for the area of the MTS illuminated.

and the largest possible area we can illuminate as:

$$D_{max} = d(1 + \pi/6) \approx 1.52d. \tag{9}$$

Finally, by using (3) with $\theta_0 = \Theta_{max}$ and $x_0 = D_{max}$, the needed HPBW to illuminate the error-free region is:

$$\text{HPBW} = \Theta_{max} = \arctan((1 + \pi/6)/2) \approx 37°. \tag{10}$$

C. ANTENNAS SYSTEM
As described in Section IIB, the sub-optimal MTS has performances similar to the ones of the optimum case if the illuminating antennas are located close to the center of the MTS and their HPBW is quite narrow to avoid illuminating the areas of the MTS where the error of the sub-optimal MTS is not negligible (see Fig. 3e-f). Therefore, it is important to design the illuminating antenna system to achieve the best performances from the proposed beamforming MTS.

In our analysis, in order to be complaint as much as possible to the 5G NR standard ETSI TR138-901 [42], the radiating system used for realizing the scanning antenna based on beamforming MTS is composed by an alignment of *half-wavelength crossed dipole antennas* (Fig. 5a) along the x direction, able to realize a scanning on the azimuthal plane. The total number of antennas is 13 and their inter-element distance is $p_x = 5.35$ mm, *i.e.,* half-wavelength at the operative frequency $f=28$ GHz. To obtain a directive radiating system illuminating the half-space in front of it, a metallic reflector of extension L=111.86 mm has been placed behind the antennas at a distance of 2.67 mm, *i.e.,* a quarter of the wavelength at the operative frequency. The scanning capabilities of the antenna on the azimuthal plane are evaluated assuming periodic boundary conditions on the $\pm y$-directions.

Using this simulation setup, we numerically evaluate the radiation performance of the illuminating source when one, two, or three crossed dipoles are active simultaneously for illuminating the MTS. The analysis is performed using the CST Microwave Studio [43]. Such a study allows identifying the minimum number of antennas required for achieving the required illumination conditions described in Section II-B.

In Fig. 5b, we compare the radiation patterns on the azimuthal plane in the three considered illumination conditions. It is clear that at least three antennas are required for achieving a HPBW close to 30° and guaranteeing the best achievable performance from the sub-optimal beamforming MTS.

D. BUILDING BEAMFORMING METASURFACE
As mentioned at the beginning of Section II, MTSs are artificial structures composed by a planar array of subwavelength unit cells, each of which performs a specific field transformation. The overall response of the MTS is defined by the spatial arrangement of such particles on the surface. In Fig. 6a, the antenna system discussed in Section III-C is combined with the proposed beamforming MTS. It is composed by 40 unit-cells along the x direction covering the entire width $D = 128.48$ mm of the antenna. The MTS is located at a distance $d = 53.53$ mm from the antenna plane. In Fig. 6c, we report the spatial phase profile of the MTS along the x direction, as described by (6). The parabolic phase profile of the phase of the transmission coefficient is mapped into the discrete number of unit-cells composing the MTS (orange dashed line, each element is highlighted by a filled dot). This curve returns the required phase that each unit cell has to exhibit in order to achieve the desired spatial profile along the MTS.

In the open technical literature, we can identify several approaches for designing the unit-cells. Following [36], each unit-cell is implemented as a cascade of three surface admittances, Y_1, Y_2, and Y_3, separated by two dielectric sheets. This configuration allows modeling each unit-cell by using its equivalent transmission line (TL) model (Fig. 6b) that returns the values of the unknown surface admittances for a desired phase of the transmission coefficient and frequency, having set unitary magnitude of the transmission coefficient, *i.e.*, fully transparent unit-cell. By considering two ROGERS DUROID/RT5870 as dielectric spacer of thickness equal to *0.787mm,* we have analytically derived the required values of the three surface admittances for each unit-cell composing the MTS.
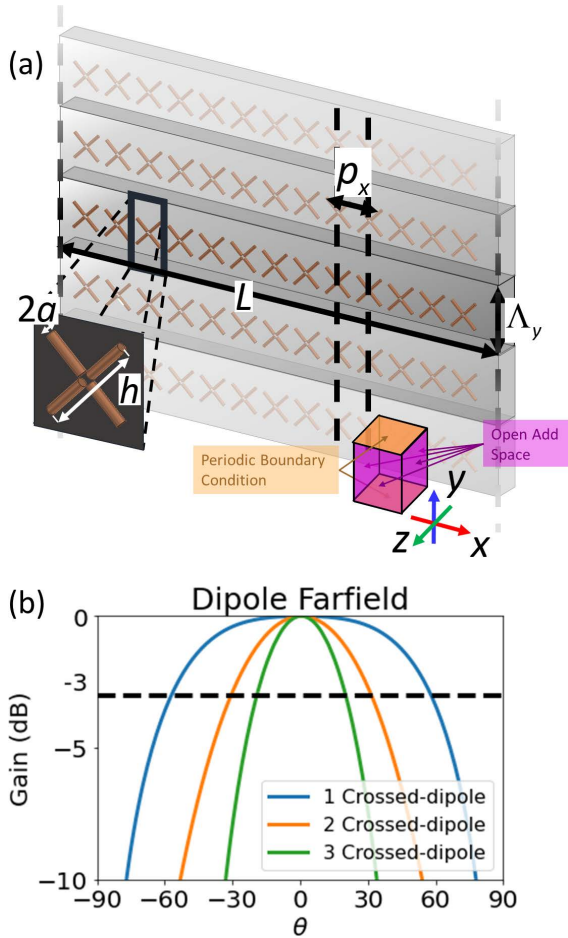
FIGURE 5. (a) Illuminating antenna system with a metallic reflector. Dimensions are: p_x = 5.35 mm, L=111.86 mm, Λ_y =10.70 mm, 2a=0.14 mm, h=4.17 mm. In the inset, the applied boundary conditions in the full-wave simulator. (b) Comparison between the radiation diagrams when one (blue line), two (orange line) and three (green line) antennas are active together.

In the Appendix, we report the design guideline and the complete set of unit cells, listing their values of the surface admittances and scattering performances in terms of complex transmission coefficients.

III. RADIATION PATTERNS

In this Section, we report the radiation performances on the azimuthal scanning plane of the proposed antenna system based on matrix beamforming MTS at the operating frequency of 28 GHz. Such radiation performances are compared to the ones achieved by the antenna array without the MTS, shown in Fig. 7a, whose scanning capabilities are enabled by a conventional BFN connected to the antennas.

In Fig. 6a, we report the scanning beams radiated by the proposed scanning antenna system based on a matrix beamforming MTS when three antennas are used simultaneously for illuminating a specific portion of the MTS. As discussed in Section II-B and II-C, this represents the best illumination condition for the MTS. The 13 antennas behind the MTS realize 11 independent beams, each of which is active when
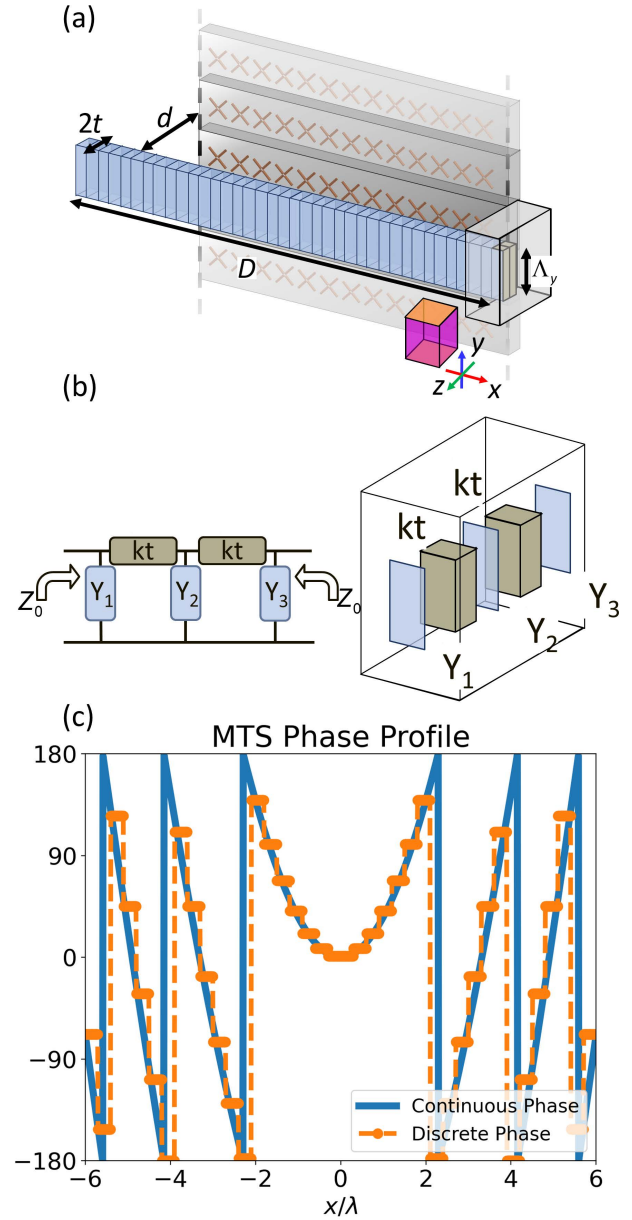

FIGURE 6. (a) Antenna system in all its components, array and MTS. Dimensions are: D=128.57mm, Λ_y = 10.70mm, 2h=3mm, d=53.53mm. (b) Equivalent transmission line model and MTS unit-cell structure; (c) Metasurface phase profile defined by Eq. (6).

three antennas are active. The 11 beams scan the FoV from $-30°$ to $+30°$ with a -3 dB scanning loss and a maximum gain of 18.12 dB at broadside. To understand the importance of the illumination conditions, in Fig. 7b, we report the scanning beams of the same antenna as in Fig. 7a, but when the 11 central antennas are active in stand-alone configuration. In this case, the illumination conditions are not optimal for the designed MTS, and the scanning capability get worse quite fast when scanning towards directions far from the broadside. However, this configuration requires that only one antenna at a time is active for generating a single beam simplifying the connectivity between the RF chains and the
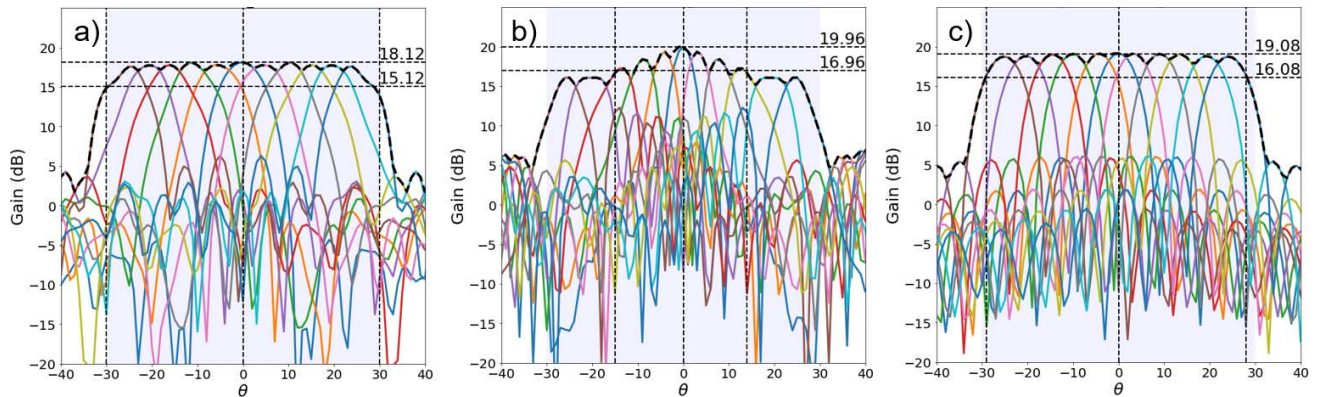
FIGURE 7. Far-field gain radiation patterns at 28 GHz: (a) MTS+array system with 3 antennas firing at the same time (MTS3ANT) (b), MTS+array system with a single antenna (MTS1ANT), and (c) a phased array with 13 antennas. In light-purple, the desired FoV is reported vs. the actual FoV in vertical black dashed-lines. While the array and the MTS3ANT have similar performances, the solution MTS1ANT is not comparable in terms of FoV.

antenna system. Finally, in Fig. 7c, we report the scanning performances of the antenna array when the beamforming MTS is removed and the scanning beams are achieved by using a conventional BFN. The performances are evaluated over the same FoV (*i.e.,* 60°). Comparing Fig. 7a and Fig. 7c, we note similar performances in terms of scanning capability and maximum directivity. However, the matrix BFN solution benefits from the advantage of radiating all the beams simultaneously when all antennas are active. This feature, in combination with good radiation performance, represents the key advantage for speeding up the IA procedure between the gNB and UE, as it will be discussed in detail in the next Sections.

IV. 5G NR IA BASED ON THE BEAMFORMING MTS-BASED SCANNING ANTENNA

The adoption of the beamforming MTS-based antenna system may benefit the IA of cellular communications, thanks to the possibility to radiate several independent beams at a time for searching the UE within the FoV of the gNB. In the following, first, we briefly review the 3GPP NR IA procedure, identifying the main phases; then, we analyze the performance when a gNB is equipped with the proposed beamforming MTS-based antenna system in both its configurations discussed in Section III: 1) when each beam is obtained by the activation of one single antenna (configuration MTS1ANT) and 2) when each beam is generated with three simultaneously activated antennas (configuration MTS3ANT).

A. 3GPP NR IA PROCEDURE

We consider a 5G NR scenario, wherein a gNB and a UE aim at establishing a connection. Upon the entrance of the UE in the cell, both the gNB and UE must find suitable transmit and receive directions to communicate in both downlink and uplink, as shown in Fig. 8. Only when a proper alignment is found, the path-loss is compensated by the directional gain and a useful signal-to-interference-plus-noise ratio (SINR)

is achieved. The 3GPP standard [44] provides a suitable mechanism to find the alignment. The procedure is based on the transmission by the gNB of a fixed number of synchronization signals, which carry system information exploited by the UE to instantiate the connection with the gNB. Each synchronization signal includes a primary synchronization signal (PSS), a secondary synchronization signal (SSS), and a physical broadcast channel (PBCH) signal. PSS and SSS are used by the receiving UE to obtain frequency and temporal synchronization, while the PBCH signal conveys fundamental network information used to allow the subsequent reception of control/data channels.

According to the 5G NR terminology, the ensemble of PSS, SSS, and PBCH is commonly referred to as synchronization signal block (SSB) and spans 240 contiguous subcarriers of 4 orthogonal frequency-division multiplexing (OFDM) symbols. Multiple SSB signals are grouped into a SSB burst, which is transmitted by the gNB in a reserved 5 ms time window with configurable periodicity of 10, 20, 40, 80, and 160 ms. The IA procedure includes four main phases [44] shown in Fig. 9:

1) *Beam sweeping*: the gNB transmits several SSBs in given spatial directions at different times covering their entire FoV.
2) *Beam measurement*: the UE employs several receive beamformers to detect the transmitted SSB. For each considered beamforming direction, the UE estimates the SINR and attempts to decode the Master Information Block (MIB) carried by the PBCH. To this end, the UE first demodulates the received waveform to *i)* decode the PSS and SSS carrying the physical-layer serving cell identifier, and *ii)* acquire information on frequency and time offsets. Subsequently, the UE decodes the PBCH. Note that, since the SSBs are spatially separated, just a few of them reach the receiver with enough power for successful MIB decoding.
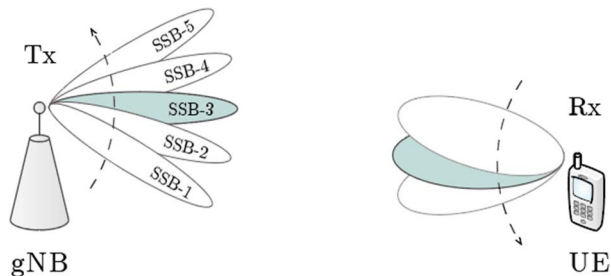3) *Beam determination*: the UE determines the pair of SSB and receiver beamformer, providing the highest

FIGURE 8. Beam sweeping procedure. Both gNB and UE search the best beam pair according to the SINR at the receiver.

FIGURE 9. IA workflow diagram showing the main steps of the procedure at both gNB and UE.

estimated SINR. The selected beamforming direction is then adopted for all subsequent transmissions and receptions at the UE.

4) *Beam reporting*: once the best beam pair is determined, the UE selects a random-access channel preamble (PRACH) to feed back to the gNB, within a configurable subset of random access (RACH) time-frequency opportunities. Since RACH opportunities are SSB-specific [45], the gNB determines the best downlink propagation direction based on the corresponding PRACH reception, alongside uplink timing of the considered UE, and other parameters.

Upon completion of the IA phase, both gNB and UE have full knowledge about the best beamformers to adopt for the forthcoming data transmission phase in the next frames.

B. IA PERFORMANCE METRICS

The decoding of the Master Information Block (MIB) carried by the PBCH is of fundamental importance during the IA procedure. The UE can acquire the information to determine the pair of SSB and receiver beamformer, providing the highest estimated SINR.

Let p_{MIB} be the probability of decoding the MIB, which is in general less than 1, due to the presence of the additive white Gaussian noise and other disturbances at the receiver. The conditional PRACH decoding probability is

$$p_{PRACH} = P(\text{PRAHC decoded}|\text{MIB decoded}). \quad (11)$$

These two quantities identify a measure of the IA downlink performance and the IA uplink performance, respectively. Furthermore, let T_{FR} be the NR frame length, and let $T_{SSB} = N_B T_{SS}$ be the length of the total SSB transmission phase, where N_B is the number of beams used for scanning and T_{SS} a single SSB duration, Note that the length of the total SSB transmission phase is strictly dependent on the number of explored directions. Indeed, the 3GPP IA procedure reported in Sec. IV-A is designed for a conventional gNB equipped with single RF chain connected to a (digital or analog) BFN, that imparts the proper excitation coefficients to the antennas composing the array. In this configuration, only one beam at a time can be radiated increasing the overall time for scanning the FoV in front of the gNB.
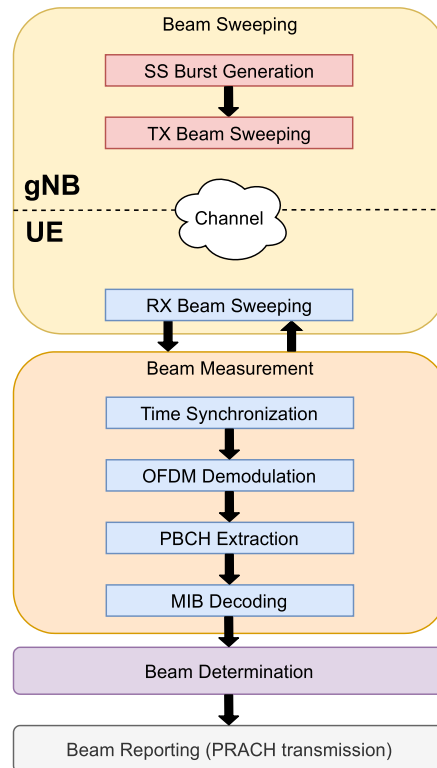
We can now define the expected MIB decoding time as:

$$\mathbb{E}[T_{MIB}] = \sum_{n=0}^{\infty} (nT_{FR} + T_{SSB})(1 - p_{MIB})^n p_{MIB}$$

$$= \frac{T_{FR} + (T_{SSB} - T_{FR})p_{MIB}}{p_{MIB}}. \quad (12)$$

Next, we discuss the adoption of the MTS-based antenna system introduced in Section II for IA in 5G NR communications. In particular, first we consider the use of the MTS1ANT and MTS3ANT solutions used at the gNB to transmit the SSB. Then, we propose a new IA protocol to fully exploit simultaneous SSB transmissions, enabled by the matrix BF-MTS antenna system.

C. MTS-ENABLED FAST IA

The proposed beamforming MTS can entirely replace the BFN. By switching the firing antenna elements, different beamforming directions are explored. In particular, using the MTS1ANT scheme a different antenna element is connected to the RF chain for each SSB transmission, while 3 antennas are connected to the RF chain simultaneously in the MTS3ANT configuration.

This implementation requires the same time of the BFN-based implementation for the transmission of the SSB. The expected MIB decoding time among changes with respect to the BFN-based implementation only due to a possibly

different probability of decoding the MIB, *i.e.,* a different value of p_{MIB}.

We now propose a modified version of the IA procedure, that may be adopted in future evolution of the standard and exploits at best the considered MTS structure. First, we observe that, differently from standard BFN implementation, the MTS implementation allows to perform multiple transmissions towards different direction simultaneously. However, this solution requires multiple RF chain operating in parallel. In this setup, for MTS1ANT, all SSBs are transmitted simultaneously, requiring one RF chain for each antenna. Instead, for MTS3ANT, three SSB transmission phases are needed to explore all directions. By connecting 3 antennas to a single RF per time, the total number of needed RF chains needed is reduced to 4, and each chain activates a different subset of antennas at each SSB transmission phase.

Moreover, the simultaneous radiation of beams towards different directions in a time significantly reduces the SSB time, that now is:

$$T_{SSB} = \begin{cases} T_{SS}, & \text{for MTS1ANT configuration} \\ 3T_{SS}, & \text{for MTS3ANT configuration,} \end{cases} \quad (13)$$

which does not depend on n_B.

To highlight the boosting introduced by the proposed system, we define the MIB decoding time gain (in percentage) as

$$G_{T_{MIB}}^{\%} = 100 \times \frac{E[T_{MIB}^{NR}] - E\left[T_{MIB}^{MTS}\right]}{E[T_{MIB}^{NR}]}, \quad (14)$$

where T_{MIB}^{NR} and T_{MIB}^{MTS} are the MIB decoding time for the 5G NR standard approach and the proposed simultaneous SSB transmission based on beamforming MTS, respectively.

We note that the radiation of more than one SSB in the FoV requires that they must be orthogonal to be properly distinguished at the receiving UE, which is not implemented yet in the standard since the orthogonality is currently achieved on time. By using semi-orthogonal pseudo-random sequences, the SINR estimation at the UE will include the effects of residual interference, considered as additional noise. Although the use of semi-orthogonal pseudo-random sequences are not standard compliant, this allows to evaluate the advantage of the proposed approach with respect to the standard one, showing that it is possible to drastically reduce the MIB decoding time.

V. 5G NR IA PERFORMANCE

In this Section, we assess the performance of the proposed MTS-based implementation. We consider a gNB communicating with a UE equipped with 4 antennas (and BFN). The channel is simulated according to the 3GPP TR 38.901 clustered-delay line (CDL) [42] model. All network devices operate at 28 GHz carrier frequency. The gNB is at cell center, with fixed rotation and 60° FoV over the azimuthal plane, whereas UEs are placed in the cell with position and azimuthal rotation chosen uniformly at random,
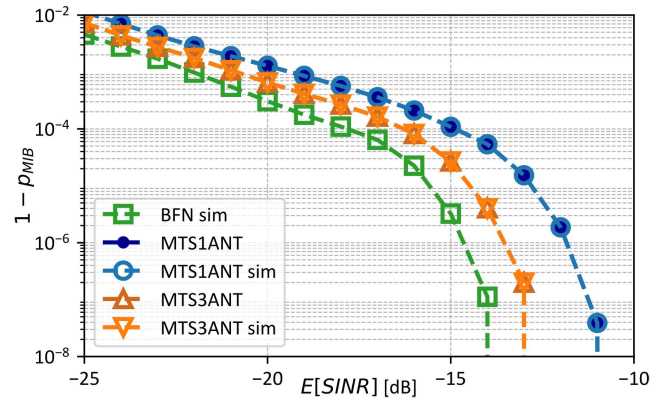

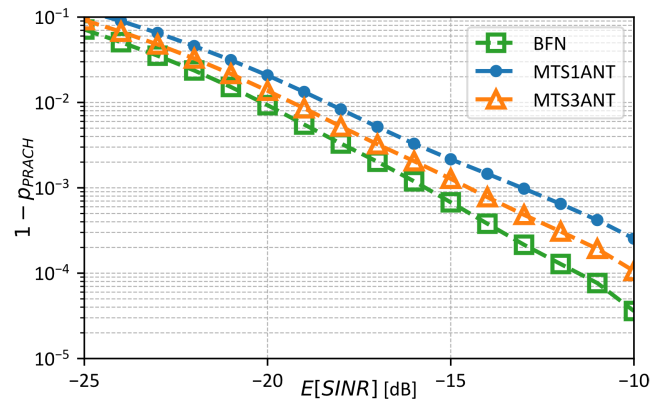**FIGURE 10.** MIB decoding error probability versus the average SINR at the UE.

FIGURE 11. PRACH decoding error probability versus the average SINR at the UE.
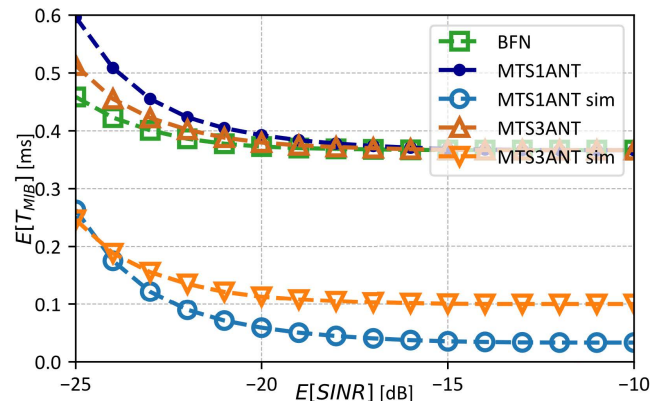

FIGURE 12. Expected MIB decoding time versus the average SINR at the UE.

with 360° FoV. Moreover, we consider 250 m inter-site distance (ISD). About the IA, we assume that *i)* the gNB generates 11 SSBs, and *ii)* only 1 RACH opportunity is available in the frequency domain for the block pattern, and *ii)* only 1 RACH opportunity is available in the frequency domain for the RACH transmission. Results presented in this section are obtained from MATLAB® simulations using the 5G Toolbox. Further simulation parameter specifications are reported in the Appendix.
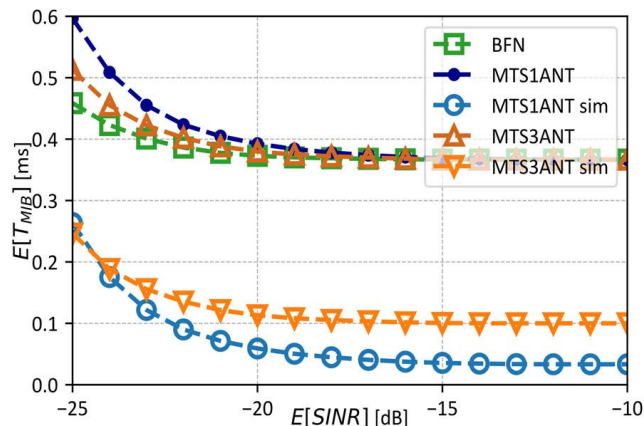
FIGURE 13. Relative MIB decoding time improvement versus the average SINR at the UE.

Fig. 10 shows the MIB decoding error probability for both the standard 5G NR IA (one SSB transmitted at a time) and the simultaneous SSB transmission, as a function of the average SINR at the UE. Results show that the MTS3ANT-based implementation performs similarly to the BFN-based implementation, while the decoding probability of the MTS1ANT-based implementation is slightly lower, as its radiation gain pattern degrades at the FOV borders, as shown in Fig. 7b. Furthermore, we observe that simultaneous SSB transmissions with semi-orthogonal pseudo-random signals do not affect the decoding probability, as the additional interference is negligible with respect to the considered noise.

Similar observations hold also for the PRACH decoding probability shown Fig. 11, which, being SSB specific, cannot be performed simultaneously. Notice that the SSB transmission phase is more robust (*i.e.*, it has a lower decoding probability), as highlighted by the higher SINR needed to perform PRACH decoding with respect to MIB decoding. Note that the MTS-based implementation performs very similar to the standard BFN-based implementation, but additionally benefitting of the simple connectivity between the RF chains and the antennas, yielding lower design complexity and costs.

Fig. 12 shows the average MIB decoding time as a function of the average SINR at the UE for all the considered implementations. We observe lower MIB decoding time for the phased array with respect to the MTS-based solutions when adopting the standard IA procedure (5G NR) as a consequence of the higher p_{MIB}. Instead, a lower MIB decoding time is experienced when adopting the simultaneous SSB transmission approach (sim). Fig. 13 shows the MIB decoding time gain (in percentage) as a function of the average SINR experienced at the UE. We observe a substantial performance improvement due to the simultaneous SSB transmissions, which, however, comes at the cost of a more complex antenna design with respect to the MTS-based standard implementation, as it requires multiple RF chains working in parallel. Nevertheless, we stress that, even with this more complex structure, the resulting antenna design provides a reduction on the number of RF chains needed to

perform beamforming, thus being still cheaper and simpler with respect to conventional BFN-based architectures.

VI. CONCLUSION
In this paper, a beamforming MTS that shifts the field manipulation from an electric level to an electromagnetic one is proposed for speeding up the initial access procedures in comparison of a standard antenna systems. We have proposed two different IA solutions: i), a very low-complexity MTS-based design allows to perform the standard 3GPP NR procedure with performance similar to the conventional BFN-based antenna arrays, and ii) a simultaneous SSB transmission paradigm can be exploited to speed up the IA, at the cost of higher hardware complexity, but still lower than conventional analog BFN architectures used for PAA. Our solution aims at embracing all the important features of a matrix BFN, parallel computing, and high-gain wide FoV scanning, while addressing its issue related to the scalability in large systems. Indeed, as demonstrated theoretically, a great advantage in using an MTS is that it design does not depends on the total number of antennas, relaxing the complexity issues typical of standard BFNs. What is important for BF-MTS is the proper illumination conditions for radiating the desired beam with a negligible scanning loss. Its capability to radiate several beams at a time has been exploited for speeding up the IA procedure in 5G NR, where the gNB is required to perform an exhaustive search for the UE within the FoV exploring all the different firing directions before starting the procedures for establishing the connection.

Here, after having reported the operative principle, design and performances of a BF-MTS, we have reported the numerical results in terms of detection probability and time, showing that a much faster IA with similar success probability can be achieved. Our system provides high gain, parallel computation, and incredible scalability for larger systems, becoming a strong contender in the NR and smart electromagnetic environment context

APPENDIX
This appendix contains a non-exhaustive guideline on how to design the unit-cells for the MTS. Here, we report what is extensively discussed in [36] but other approaches are possible [46]. Moreover, it contains further information on the simulation setup.

A. UNIT CELLS IDEAL SURFACE IMPEDANCES
With reference to Fig.6b each unit-cell can be modelled with a transmission line approach. In this sense, each element of the unit-cell, surface impedance, and dielectric substrate has a straightforward counterpart in the transmission line model, shunt admittance and line segment respectively, as shown in Fig.6b. By this means, an arbitrary arrangement of dielectric material and surface impedances can be described effectively by a transmission line model. The goal of a refractive MTS is to have as less reflection as possible while maintaining high transmission and phase manipulation capabilities. These

properties can be summarized for the unit-cell in zero reflection, unitary transmission, and arbitrary phase-shift. Now, by referring to the scattering coefficients of the S-matrix

$$S = \begin{bmatrix} s_{11} & s_{12} \\ s_{21} & s_{22} \end{bmatrix}, \quad (A1)$$

we obtain the system of equations

$$\begin{cases} s_{11} = 0 \\ |s_{12}| = 1 \\ \arg(s_{12}) = \phi, \end{cases} \quad (A2)$$

where ϕ is an arbitrary phase. For a deeper analysis of the problem see [47]. At this point, it is necessary to find the S-matrix (A1) for the transmission line model to be able to apply (A2). Directly evaluating the S-matrix for a cascade of components is often challenging and at best tedious. A well-known result in microwave theory [48] is that a cascade of transmission line elements can be easily modeled by the transmission matrix, or ABCD matrix. The ABCD matrix allows the description of a complex cascade of elements just by evaluating the product between the ABCD matrices of the single components. Once the matrix of the cascade is found, it is possible to convert this result directly to the S-matrix we wanted at the beginning [49].

This general approach can be particularized for the problem of the unit-cells in (A2). Having three-equations we need three different degree of freedom, which are provided by three surface admittances $Y_i = 1/Z_i$ with $i = 1, 2, 3$, giving that the cell thickness is fixed by design. Following the procedure briefly explained in the previous lines, (A2) can be solved for the three admittances directly [47] or numerically. Table 1 reports the set of impedances for each value of phase we needed for the discretization of the phase-profile. We report only one side of the MTS, discretized in 20 unit-cells, being the system completely symmetric, as shown in Fig. 6c.

B. SIMULATION PARAMETERS

We consider the standard NR frame length $T_{FR} = 10$ ms, with each frame split into 10 subframes of 8 slots each. Within the OFDM modulation a 512-sized discrete Fourier transform is applied. The sampling rate is 61.44 MHz, and 14 OFDM symbols can be transmitted per slot. For the IA, we adopt the "Case D" SSB block pattern [44]. which implies a subcarrier spacing of 120 kHz. For the channel model, we consider an urban micro-cell (Umi) scenario wherein the devices are in line-of-sight (LoS), and the shadowing is neglected. The path loss and the channel matrix is computed according to the procedure illustrated in [42].

TABLE 1. Surface impedances and transmission coefficients of the unit-cell composing the beamforming MTS.

Unit cell no.	Surface impedances (Z1, Z2, Z3) [Ohm/sq.]	Transmission coefficient (Mag., Phase) [lin.; Degrees]
1	(1796, 446, 1796)	(0.9998, -68)
2	(-268, 1915, -268)	(0.9998, -152)
3	(-174, -52, -174)	(0.9998, 125)
4	(-106, -44, -106)	(0.9999, 45)
5	(77, -191, 77)	(0.9998, -32)
6	(-445, 192, -445)	(0.9997, -108)
7	(-226, -175, -266)	(0.9997, 180)
8	(-163, -46, -163)	(0.9997, 111)
9	(-106, -44, -106)	(0.9999, 45)
10	(6, -110, 6)	(0.9998, -17)
11	(-5908, 309, -5908)	(0.9998, -75)
12	(-328, 254, -328)	(0.9996, -129)
13	(-228, -191, -228)	(0.9999, -178)
14	(-186, -62, -186)	(0.9999, 139)
15	(-155, -43, -155)	(0.9997, 100)
16	(-128, -41, -128)	(0.9998, 68)
17	(-102, -46, -102)	(0.9997, 41)
18	(-77, -54, -77)	(0.9997, 21)
19	(-56, -65, -56)	(0.9997, 8)
20	(-42, -73, -42)	(0.9999, 1)

REFERENCES

[1] A. Gupta and R. K. Jha, "A survey of 5G network: Architecture and emerging technologies," *IEEE access*, vol. 3, pp. 1206–1232, 2015, doi: 10.1109/ACCESS.2015.2461602.

[2] S.-Y. Lien, S.-L. Shieh, Y. Huang, B. Su, Y.-L. Hsu, and H.-Y. Wei, "5G new radio: Waveform, frame structure, multiple access, and initial access," *IEEE Commun. Mag.*, vol. 55, no. 6, pp. 64–71, Jun. 2017, doi: 10.1109/MCOM.2017.1601107.

[3] Z. Zhang, Y. Xiao, Z. Ma, M. Xiao, Z. Ding, X. Lei, G. K. Karagiannidis, and P. Fan, "6G wireless networks: Vision, requirements, architecture, and key technologies," *IEEE Veh. Technol. Mag.*, vol. 14, no. 3, pp. 28–41, Sep. 2019, doi: 10.1109/MVT.2019.2921208.

[4] M. Giordani, M. Polese, M. Mezzavilla, S. Rangan, and M. Zorzi, "Toward 6G networks: Use cases and technologies," *IEEE Commun. Mag.*, vol. 58, no. 3, pp. 55–61, Mar. 2020, doi: 10.1109/MCOM.001.1900411.

[5] M. Giordani, M. Mezzavilla, and M. Zorzi, "Initial access in 5G mmWave cellular networks," *IEEE Commun. Mag.*, vol. 54, no. 11, pp. 40–47, Nov. 2016, doi: 10.1109/MCOM.2016.1600193CM.

[6] H. Soleimani, R. Parada, S. Tomasin, and M. Zorzi, "Fast initial access for mmWave 5G systems with hybrid beamforming using online statistics learning," *IEEE Commun. Mag.*, vol. 57, no. 9, pp. 132–137, Sep. 2019, doi: 10.1109/MCOM.2019.1800805.

[7] S. Tomasin, C. Mazzucco, D. De Donno, and F. Cappellaro, "Beam-sweeping design based on nearest users position and beam in 5G mmWave networks," *IEEE Access*, vol. 8, pp. 124402–124413, 2020, doi: 10.1109/ACCESS.2020.3006015.

[8] J. S. Herd and M. D. Conway, "The evolution to modern phased array architectures," *Proc. IEEE*, vol. 104, no. 3, pp. 519–529, Mar. 2016, doi: 10.1109/JPROC.2015.2494879.

[9] P. Rocca, L. Poli, A. Polo, and A. Massa, "Optimal excitation matching strategy for sub-arrayed phased linear arrays generating arbitrary-shaped beams," *IEEE Trans. Antennas Propag.*, vol. 68, no. 6, pp. 4638–4647, Jun. 2020, doi: 10.1109/TAP.2020.2972641.

[10] P. Rocca, G. Oliveri, R. J. Mailloux, and A. Massa, "Unconventional phased array architectures and design methodologies—A review," *Proc. IEEE*, vol. 104, no. 3, pp. 544–560, Mar. 2016, doi: 10.1109/JPROC.2015.2512389.

[11] R. Haupt, "Reducing grating lobes due to subarray amplitude tapering," in *Proc. Antennas Propag. Soc. Int. Symp.*, Jun. 1985, pp. 119–122, doi: 10.1109/aps.1985.1149384.

[12] S. Mosca, F. Bilotti, A. Toscano, and L. Vegni, "A novel design method for Blass matrix beam-forming networks," *IEEE Trans. Antennas Propag.*, vol. 50, no. 2, pp. 225–232, Aug. 2002, doi: 10.1109/8.997999.

[13] H. Ren, H. Zhang, Y. Jin, Y. Gu, and B. Arigong, "A novel 2-D 3 × 3 nolen matrix for 2-D beamforming applications," *IEEE Trans. Microw. Theory Techn.*, vol. 67, no. 11, pp. 4622–4631, Nov. 2019, doi: 10.1109/TMTT.2019.2917211.

[14] A. K. Vallappil, M. K. A. Rahim, B. A. Khawaja, N. A. Murad, and M. M. Gajibo, "Butler matrix based beamforming networks for phased array antenna systems: A comprehensive review and future directions for 5G applications," *IEEE Access*, vol. 9, 2020, doi: 10.1109/ACCESS.2020.3047696.

[15] M. Giordani, M. Polese, A. Roy, D. Castor, and M. Zorzi, "A tutorial on beam management for 3GPP NR at mmWave frequencies," *IEEE Commun. Surveys Tuts.*, vol. 21, no. 1, pp. 173–196, 1st Quart., 2018, doi: 10.1109/COMST.2018.2869411.

[16] O. Quevedo-Teruel, H. Chen, A. Díaz-Rubio, G. Gok, A. Grbic, G. Minatti, E. Martini, S. Maci, G. V. Eleftheriades, M. Chen, and N. I. Zheludev, "Roadmap on metasurfaces," *J. Opt.*, vol. 21, no. 7, Jul. 2019, Art. no. 073002, doi: 10.1088/2040-8986/AB161D.

[17] M. Bodehou, E. Martini, S. Maci, I. Huynen, and C. Craeye, "Multi-beam and beam scanning with modulated metasurfaces," *IEEE Trans. Antennas Propag.*, vol. 68, no. 3, pp. 1273–1281, Mar. 2020, doi: 10.1109/TAP.2019.2944554.

[18] M. Faenzi, D. Gonzalez-Ovejero, and S. Maci, "Flat gain broadband metasurface antennas," *IEEE Trans. Antennas Propag.*, vol. 69, no. 4, pp. 1942–1951, Apr. 2021, doi: 10.1109/TAP.2020.3026476.

[19] E. Martini and S. Maci, "Modulated metasurfaces for microwave field manipulation: Models, applications, and design procedures," *IEEE J. Microw.*, vol. 2, no. 1, pp. 44–56, Jan. 2022, doi: 10.1109/JMW.2021.3126199.

[20] A. Monti, J. Soric, M. Barbuto, D. Ramaccia, S. Vellucci, F. Trotta, A. Alu, A. Toscano, and F. Bilotti, "Mantle cloaking for co-site radio-frequency antennas," *Appl. Phys. Lett.*, vol. 108, no. 11, Mar. 2016, Art. no. 113502, doi: 10.1063/1.4944042.

[21] A. Monti, J. Soric, A. Alù, F. Bilotti, A. Toscano, and L. Vegni, "Overcoming mutual blockage between neighboring dipole antennas using a low-profile patterned metasurface," *IEEE Antennas Wireless Propag. Lett.*, vol. 11, pp. 1414–1417, 2012, doi: 10.1109/LAWP.2012.2229102.

[22] S. Vellucci, A. Monti, M. Barbuto, A. Toscano, and F. Bilotti, "Satellite applications of electromagnetic cloaking," *IEEE Trans. Antennas Propag.*, vol. 65, no. 9, pp. 4931–4934, Sep. 2017, doi: 10.1109/TAP.2017.2722865.

[23] M. Barbuto, Z. Hamzavi-Zarghani, M. Longhi, A. Monti, D. Ramaccia, S. Vellucci, A. Toscano, and F. Bilotti, "Metasurfaces 3.0: A new paradigm for enabling smart electromagnetic environments," *IEEE Trans. Antennas Propag.*, early access, Dec. 1, 2021, doi: 10.1109/TAP.2021.3130153.

[24] O. Özdogan, E. Björnson, and E. G. Larsson, "Intelligent reflecting surfaces: Physics, propagation, and pathloss modeling," *IEEE Wireless Commun. Lett.*, vol. 9, no. 5, pp. 581–585, May 2020, doi: 10.1109/LWC.2019.2960779.

[25] Y.-C. Liang, R. Long, Q. Zhang, J. Chen, H. V. Cheng, and H. Guo, "Large intelligent surface/antennas (LISA): Making reflective radios smart," 2019, *arXiv:1906.06578*.

[26] M. Barbuto, Z. Hamzavi-Zarghani, M. Longhi, A. V. Marini, A. Monti, D. Ramaccia, S. Vellucci, A. Toscano, and F. Bilotti, "Intelligence enabled by 2D metastructures in antennas and wireless propagation systems," *IEEE Open J. Antennas Propag.*, vol. 3, pp. 135–153, 2022, doi: 10.1109/OJAP.2021.3138617.

[27] V. S. Asadchy, M. Albooyeh, S. N. Tcvetkova, A. Díaz-Rubio, Y. Ra'di, and S. A. Tretyakov, "Perfect control of reflection and refraction using spatially dispersive metasurfaces," *Phys. Rev. B, Condens. Matter*, vol. 94, no. 7, Aug. 2016, Art. no. 075142, doi: 10.1103/PhysRevB.94.075142.

[28] S. Tretyakov, *Analytical Modeling in Applied Electromagnetics*. Norwood, MA, USA: Artech House, 2003.

[29] J. P. S. Wong, A. Epstein, and G. V. Eleftheriades, "Reflectionless wide-angle refracting metasurfaces," *IEEE Antenn. Wireless Propag. Lett.*, vol. 15, pp. 1293–1296, 2016, doi: 10.1109/LAWP.2015.2505629.

[30] D. Ramaccia, D. L. Sounas, A. Alu, A. Toscano, and F. Bilotti, "Phase-induced frequency conversion and Doppler effect with time-modulated metasurfaces," *IEEE Trans. Antennas Propag.*, vol. 68, no. 3, pp. 1607–1617, Mar. 2020, doi: 10.1109/TAP.2019.2952469.

[31] D. Ramaccia, D. L. Sounas, A. V. Marini, A. Toscano, and F. Bilotti, "Electromagnetic isolation induced by time-varying metasurfaces: Non-reciprocal Bragg grating," *IEEE Antennas Wireless Propag. Lett.*, vol. 19, no. 11, pp. 1886–1890, Nov. 2020, doi: 10.1109/lawp.2020.2996275.

[32] A. V. Marini, D. Ramaccia, A. Toscano, and F. Bilotti, "Metasurface virtual absorbers: Unveiling operative conditions through equivalent lumped circuit model," *EPJ Appl. Metamater.*, vol. 8, p. 3, Jan. 2021, doi: 10.1051/epjam/2020014.

[33] A. V. Marini, D. Ramaccia, A. Toscano, and F. Bilotti, "Metasurface-bounded open cavities supporting virtual absorption: Free-space energy accumulation in lossless systems," *Opt. Lett.*, vol. 45, no. 11, pp. 3147–3150, May 2020, doi: 10.1364/ol.389389.

[34] S. Vellucci, A. Monti, M. Barbuto, A. Toscano, and F. Bilotti, "Waveform-selective mantle cloaks for intelligent antennas," *IEEE Trans. Antennas Propag.*, vol. 68, no. 3, pp. 1717–1725, Mar. 2020, doi: 10.1109/TAP.2019.2948736.

[35] A. Epstein and G. V. Eleftheriades, "Passive lossless Huygens metasurfaces for conversion of arbitrary source field to directive radiation," *IEEE Trans. Antennas Propag.*, vol. 62, no. 11, pp. 5680–5695, Nov. 2014, doi: 10.1109/TAP.2014.2354419.

[36] M. Chen, E. Abdo-Sánchez, A. Epstein, and G. V. Eleftheriades, "Theory, design, and experimental verification of a reflectionless bianisotropic Huygens' metasurface for wide-angle refraction," *Phys. Rev. B, Condens. Matter*, vol. 97, no. 12, pp. 1–16, Mar. 2018, doi: 10.1103/PhysRevB.97.125433.

[37] V. G. Ataloglou and G. V. Eleftheriades, "Arbitrary wave transformations with Huygens' metasurfaces through surface-wave optimization," 2021, *arXiv:2106.07109*.

[38] C. A. Balanis, *Antenna Theory: Analysis and Design*. Hoboken, NJ, USA: Wiley, 2005.

[39] A. Kalvach and Z. Szabó, "Aberration-free flat lens design for a wide range of incident angles," *J. Opt. Soc. Amer. B, Opt. Phys.*, vol. 33, no. 2, p. A66, Feb. 2016, doi: 10.1364/josab.33.000a66.

[40] M. Born and E. Wolf, "Principles of optics: Electromagnetic theory of propagation, interference and diffraction of light," *Princ. Opt.*, to be published, doi: 10.1017/CBO9781139644181.

[41] X. Luo, F. Zhang, M. Pu, Y. Guo, X. Li, and X. Ma, "Recent advances of wide-angle metalenses: Principle, design, and applications," *Nanophotonics*, vol. 11, no. 1, pp. 1–20, Dec. 2021, doi: 10.1515/nanoph-2021-0583.

[42] *5G; Study on Channel Model for Frequencies From 0.5 to 100 GHz*, Standard TSGR, TR 138 901 V16.1.0, (3GPP TR 38.901 Version 16.1.0 Release 16), 2020.

[43] *CST Studio Suite 3D EM Simulation and Analysis Software*.

[44] *5G; NR; Physical Layer Procedures for Data*, Standard TSGR, TS 138 214 V16.2.0, 3GPP TS 38.214 Version 16.2.0 Release 16, 2020.

[45] *5G; NR; Medium Access Control (MAC) Protocol Specification*, Standard TSGR, TS 138 321 V16.1.0, 3GPP TS 38.321 Version 16.1.0 Release 16, 2020.

[46] E. F. Kuester, M. A. Mohamed, M. Piket-May, and C. L. Holloway, "Averaged transition conditions for electromagnetic fields at a metafilm," *IEEE Trans. Antennas Propag.*, vol. 51, no. 10, pp. 2641–2651, Oct. 2003, doi: 10.1109/TAP.2003.817560.

[47] A. Epstein and G. V. Eleftheriades, "Arbitrary power-conserving field transformations with passive lossless omega-type bianisotropic metasurfaces," *IEEE Trans. Antennas Propag.*, vol. 64, no. 9, pp. 3880–3895, Sep. 2016, doi: 10.1109/TAP.2016.2588495.

[48] D. M. Pozar, *Microwave Engineering*, 2011.

[49] D. A. Frickey, "Conversions between S, Z, Y, H, ABCD, and T parameters which are valid for complex source and load impedances," *IEEE Trans. Microw. Theory Techn.*, vol. 42, no. 2, pp. 205–211, Feb. 1994.

LUCA STEFANINI was born in Rome, Italy, in 1996. He received the bachelor's degree in electronic engineering and the master's degree in electronic engineering for industry and innovation from Roma Tre University, in November 2018 and March 2021, respectively, where he is currently pursuing the Ph.D. degree in applied electronics. His research interests include metasurface and metamaterial field, spanning from metasurface for antenna systems to temporal metamaterials.

ALBERTO RECH (Graduate Student Member, IEEE) was born in Montebelluna, Italy, in 1996. He received the bachelor's degree in information engineering and the master's degree in ICT for internet and multimedia engineering from the University of Padova, Italy, in 2018 and 2020, respectively, and the master's degree in communication engineering from the National Taiwan University, in August 2020. He is currently pursuing the Ph.D. degree in information engineering with the University of Padova. His research interests include signal processing and protocol design for smart electromagnetic environment systems and access schemes for machine-type communications.

STEFANO TOMASIN (Senior Member, IEEE) received the Ph.D. degree in telecommunications engineering from the University of Padova, Italy, in 2003. In 2002, he joined the University of Padova, where he is currently an Associate Professor. He was on leave at Philips Research, Eindhoven, The Netherlands, in 2002; Qualcomm Research Laboratories, San Diego, CA, USA, in 2004; Polytechnic University, Brooklyn, NY, USA, in 2007; and the Huawei Mathematical and Algorithmic Sciences Laboratory, Boulogne-Billancourt, France, in 2015. His current research interests include physical layer security and signal processing for wireless communications, with application to cellular systems. He was an Editor of the IEEE TRANSACTIONS ON VEHICULAR TECHNOLOGY, from 2011 to 2017; an Editor of IEEE TRANSACTIONS ON SIGNAL PROCESSING, from 2017 to 2021; and has been an Editor of the IEEE TRANSACTIONS ON INFORMATION FORENSICS AND SECURITY, since 2020. Since 2011, he has also been an Editor of *EURASIP Journal on Wireless Communications and Networking*.

DAVIDE RAMACCIA (Senior Member, IEEE) received the B.S. and M.S. degrees *(summa cum laude)* in electronic and ICT engineering and the Ph.D. degree in electronic engineering from Roma Tre University, Rome, Italy, in 2007, 2009, and 2013, respectively.

He was with the Department of Engineering, from 2013 to 2021, and has been with the Department of Industrial, Electronic, and Mechanical Engineering, since 2021, with Roma Tre University. He has coauthored more than 100 articles in international journals, conference proceedings, book chapters, and holds one patent. His main research interests include the modeling and design of (space–)time-varying metamaterials and metasurfaces and their applications to microwave components and antennas, and the analysis of anomalous scattering effects in temporal metamaterials. Since 2015, he has been serving as a member for the Steering Committee of the International Congress on Advanced Electromagnetic Materials in Microwaves and Optics—Metamaterials Congress. In 2022, he was appointed as a member of the IEEE APS Award Committee by the IEEE APS Society. He is a member of the Technical Program Committee of the International Congress on Laser Science and Photonics Applications—CLEO 2022. He has been serving the scientific community, by playing roles in the management of scientific societies, in the editorial board of international journals, and in the organization of conferences and courses. He was the recipient of a number of awards and recognitions, including The Electromagnetics Academy Young Scientist Award, in 2019; seven Outstanding Reviewer Award by the IEEE TRANSACTIONS ON ANTENNAS AND PROPAGATION, from 2013 to 2021; the IET prizes for the Best Poster on Microwave Metamaterials, in 2013; and the IET Award for the Best Poster on the Metamaterial Application in antenna field, in 2011. He is currently the General Secretary of the Virtual Institute for Artificial Electromagnetic Materials and Metamaterials (METAMORPHOSE VI, the International Metamaterials Society) and has been an Elected Member of the Board of Directors of the same association from three consecutive terms, since 2014. He was also a guest co-editor of three special issues on metamaterials and metasurfaces and a Lead Guest-Editor for the Special Cluster on Metadome for Antenna Systems of IEEE ANTENNAS AND WIRELESS PROPAGATION LETTERS, in 2022. He has been the General Chair and a Local Organizer of the 39th and 42nd EUPROMETA Doctoral School on Metamaterials held in Rome, in 2019 and 2021, respectively. He has been a Technical Program Coordinator (Track ''Electromagnetics and Materials'') for the 2016 IEEE Antennas and Propagation Symposium. He was elected as a Secretary of the Project Management Board of the H2020 CSA Project Nanoarchitectronics, from 2017 to 2018. He serves as an Associate Editor for IEEE ACCESS, since 2019; a Scientific Moderator for IEEE TechRxiv, since 2019; and a technical reviewer for the major international journals related to electromagnetic field theory and metamaterials.

ALESSANDRO TOSCANO (Senior Member, IEEE) was born in Capua, in 1964. He graduated in electronic engineering from the Sapienza University of Rome, in 1988, and received the Ph.D. degree, in 1993.

Since 2011, he has been a Full Professor of electromagnetic fields with the Engineering Department, Roma Tre University. He carries out an intense academic and scientific activity, both nationally and internationally. He is the author of more than 100 publications in international journals indexed ISI or Scopus; of these on a worldwide scale, three are in the first 0.1 percentile, five in the first 1 percentile, and 25 in the first 5 percentile in terms of number of quotations and journal quality.

Prof. Toscano was a member of Roma Tre University Academic Senate, from April 2013 to January 2018. From October 2016 to October 2018, he was a member of the National Commission which enables National Scientific Qualifications to Full and Associate Professors in the tender sector 09/F1—electromagnetic fields. He is currently a member of the Board of Director of Radiolabs (a non-for-profit Research Consortium), of the Steering Committee of the National Competence Center on Cyber 4.0 and the Scientific Council of CIRIAF (Interuniversity Research Center on Pollution and the Environment). Since January 2018, he has been the Vice-Rector for Innovation and Technology Transfer. In addition to his commitment in organizing scientific events, he also carries out an intense editorial activity as a member of the review committees of major international journals and conferences in the field of applied electromagnetics. He has held numerous invited lectures at universities, public, and private research institutions; and national and international companies on the subject of artificial electromagnetic materials, metamaterials, and their applications. He actively participated in founding the international association on metamaterials Virtual Institute for Advanced Electromagnetic Materials—METAMORPHOSE VI. He coordinates and participates in several research projects and contracts funded by the national and international public and private research institutions and industries. His scientific research has as ultimate objective the conceiving, designing, and manufacturing of innovative electromagnetic components with a high technological content that show enhanced performance compared to those obtained with traditional technologies and that respond to the need for environment and human health protection. His research interests include metamaterials and unconventional materials, in collaboration with Professor A. Alù's Group at The University of Texas at Austin, USA, research and development of electromagnetic cloaking devices and their applications (First place winner of the Leonardo Group Innovation Award for the research project entitled: ''Metamaterials and electromagnetic invisibility'') and the research and manufacturing of innovative antenna systems and miniaturized components (first place winner of the Leonardo Group Innovation Award for the research project entitled: ''Use of metamaterials for miniaturization of components''—MiniMETRIS).

FEDERICO MORETTO was born in Bassano del Grappa, Italy. He received the bachelor's degree in computer engineering and the master's degree in ICT for internet and multimedia engineering from the University of Padova, Italy, in 2018 and 2020, respectively. From 2011 to 2013, he worked as a Software Developer with CLS Development. From 2013 to 2018, he was a Designer and Programmer with the Squared Laboratory. In 2021, he was with the Department of Information Engineering, University of Padova, where he worked on intelligent reflective surfaces (IRSs). Since 2022, he has been with NTT Data Italia, where he works as a Technical Engineer. His research interest includes telecommunications systems.

FILIBERTO BILOTTI (Fellow, IEEE) received the Laurea and Ph.D. degrees in electronic engineering from Roma Tre University, Rome, Italy, in 1998 and 2002, respectively.

He was with the Faculty of Engineering, from 2002 to 2012; and the Department of Engineering, from 2013 to 2021; and has been with the Department of Industrial, Electronic, and Mechanical Engineering, since 2021, with Roma Tre University, where he serves as a Full Professor of electromagnetic field theory, since 2014; and the Director of the Antennas and Metamaterials Research Laboratory, since 2012. His main research interests include the analysis and design of microwave antennas and arrays and analytical modeling of artificial electromagnetic materials, metamaterials, and metasurfaces, including their applications at both microwave and optical frequencies. In the last ten years, his main research interests include the analysis and design of cloaking metasurfaces for antenna systems; on the modeling and applications of (space and) time-varying metasurfaces; on the topological-based design of antennas supporting structured field; on the modeling, design, implementation, and application of reconfigurable metasurfaces; on the concept of meta-gratings and related applications in optics and at microwaves; and on the modeling and applications of optical metasurfaces. The research activities developed in the last 20 years has resulted in more than 570 papers in international journals, conference proceedings, book chapters, and three patents.

Prof. Bilotti was the recipient of a number of awards and recognitions, including the elevation to the IEEE Fellow Grade for contributions to metamaterials for electromagnetic and antenna applications, in 2017; the Outstanding Associate Editor of the IEEE TRANSACTIONS ON ANTENNAS AND PROPAGATION, in 2016; the NATO SET Panel Excellence Award, in 2016; the Finmeccanica Group Innovation Prize, in 2014; the Finmeccanica Corporate Innovation Prize, in 2014; the IET Best Poster Paper Award (Metamaterials 2013 and Metamaterials 2011); and the Raj Mittra Travel Grant Senior Researcher Award, in 2007. He has been serving the scientific community, by playing leading roles in the management of scientific societies, in the editorial board of international journals, and in the organization of conferences and courses. In particular, he was a Founding Member of the Virtual Institute for Artificial Electromagnetic Materials and Metamaterials—METAMORPHOSE VI, in 2007. He was elected as a member of the Board of Directors of the Same society for two terms, from 2007 to 2013; and as the President for two terms, from 2013 to 2019. He currently serves the METAMORPHOSE VI as the Vice President and has been the Executive Director, since 2019. He served/serves as a member of the Editorial Board for the *International Journal of RF and Microwave Computer-Aided Engineering*, from 2009 to 2015; *Nature Scientific Reports*, from 2013 to 2016; and *EPJ Applied Metamaterials*, since 2013. In 2007, he hosted the inaugural edition of the International Congress on Advanced Electromagnetic Materials in Microwaves and Optics—Metamaterials Congress, served as the Chair for the Steering Committee of the same conference for eight editions (from 2008 to 2014 and in 2019); and was elected as the General Chair of the Metamaterials Congress, from 2015 to 2018. He was also the General Chair of the Second International Workshop on Metamaterials-by-Design Theory, Methods, and Applications to Communications and Sensing, in 2016; and has been serving as the chair or a member for the technical program, steering, and organizing committee of the main national and international conferences in the field of applied electromagnetics. He was also the guest editor of five special issues in international journals. He served as an Associate Editor for the *Metamaterials*, from 2007 to 2013; and the IEEE TRANSACTIONS ON ANTENNAS AND PROPAGATION, from 2013 to 2017.

● ● ●